Available online at www.sciencedirect.com
SCIENCE DIRECT
Journal of Chromatography A, 1095 (2005) 16–26
JOURNAL OF CHROMATOGRAPHY A
www.elsevier.com/locate/chroma

Predictive modeling of protein adsorption along the bed height by taking into account the axial nonuniform liquid dispersion and particle classification in expanded beds

Junxian Yun [1], Dong-Qiang Lin, Shan-Jing Yao *

Department of Chemical and Biochemical Engineering, Zhejiang University, ZheDa Road 38, Hangzhou 310027, PR China

Received 8 May 2005; received in revised form 22 July 2005; accepted 25 July 2005
Available online 18 August 2005

Abstract

Expanded bed adsorption (EBA) is a special chromatography technique with perfect classification of adsorbent particles in the column, thus the performance of protein adsorption in expanded beds is particular, obviously nonuniform and complex along the column. Detailed description of the complex adsorption kinetics of proteins in expanded bed is essential for better analyzing of adsorptive mechanisms, the design of chromatographic processes and the optimization of operation parameters of EBA processes. In this work, a theoretical model for the prediction of protein adsorption kinetics in expanded beds was developed by taking into account the classified distribution of adsorbent particles along the bed height, the nonuniform behaviors of axial liquid dispersion, the axial variation of local bed voidage as well as the axial changes of target component mass transfer. The model was solved using the implicit finite difference scheme combining with the orthogonal collocation method, and then applied to predict the breakthrough behaviors of bovine serum albumin (BSA) on Streamline DEAE and lysozyme on Streamline SP along the bed height in expanded beds under various conditions. In addition, the experiments of front adsorption of BSA on Streamline DEAE at different axial column positions were carried out to reveal the adsorption kinetics of BSA along the bed height in a 20 mm I.D. expanded bed, and the influences of liquid velocity and feed concentration on the breakthrough behaviors were also analyzed. The breakthrough behaviors predicted by the present model were compared with the experimental data obtained in this work and in the literature published. The agreement between the prediction and the experimental breakthrough curves is satisfied.

Keywords: Expanded bed adsorption; Protein adsorption; Mathematical model; Particle size distribution; Axial liquid dispersion; Local voidage

1. Introduction

Expanded bed adsorption (EBA) has received much attention as one of the most effective techniques for purification of target biomolecules directly from unclarified feedstocks with cells or cell debris in downstream processes [1–4]. The adsorbent particles used in EBA processes always have various sizes and densities, which cause perfectly classified distribution of adsorbent particles along the bed height, corresponding nonuniform behaviors of liquid dispersion, local bed voidage as well as biomolecule adsorption performance [5–13]. Due to the influences of fluid hydrodynamics, particle classification and target component transfer, the analysis of adsorption kinetics in EBA is complex. Detailed modeling of the adsorption performance in expanded beds is fundamental and crucial to the better understanding of the adsorptive behaviors, the design of EBA processes, the optimization of operation parameters and the design of adsorbents and column systems.

Several models have been suggested to describe the protein adsorption behaviors in EBA. Wiblin et al. [14] used the well-established fixed-bed adsorption model to simulate the adsorption performance of α-amylase in EBA. In their model, the mean diameter of adsorbent particles, the axial dispersion coefficient of liquid, the local bed voidage as well as the solid–liquid mass transfer coefficient were assumed

* Corresponding author. Tel.: +86 571 87951982; fax: +86 571 87951015.
[1] Present address: College of Chemical Engineering and Materials Science, Zhejiang University of Technology, Hangzhou 310014, PR China.

0021-9673/$ – see front matter © 2005 Published by Elsevier B.V.
doi:10.1016/j.chroma.2005.07.120

to be constant. Bruce and Chase [15] modified this model to analyze the breakthrough curves of BSA and lysozyme by considering the variations of bed voidage and axial liquid dispersion coefficient with the experimental data, but the axial variation of particle size was neglected. Wright and Glasser [16] developed a protein adsorption model for liquid–solid fluidized beds taking into account in-bed hydrodynamics, solid-phase dispersion and mass transfer characteristics. Tong et al. [17] and Chen et al. [18] also used this model to describe lysozyme purification and BSA adsorption performance. Similarly, the axial variation of particle size was also neglected. Tong et al. [19] suggested a modified model using an empirical correlation of the axial variation of particle size, but ignored the axial variation of bed voidage. Li et al. [20] proposed a model by dividing an expanded bed into three zones based on the experimental results by Bruce and Chase [7]. In those three zones, different experimental values of particle diameter, bed voidage and axial liquid dispersion coefficient were directly used. Their model was efficient in analysis of the influence of parameters on the breakthrough curves of lysozyme in the expanded bed. Kaczmarski and Bellot [21] presented an improved theoretical model, in which the axial and the local variations of particle diameter, the axial variation of bed voidage, and the axial variation of solid–liquid mass transfer coefficient were taken into account, but the variation of axial liquid dispersion coefficient was neglected. In their recent work [22], the influence of particle size distribution was also considered by employing an empirical correlation obtained by Tong and Sun [8]. In these models mentioned above, priori bed expansion height should be given before the calculation of the adsorption behaviors because its values at different operation conditions cannot be determined directly from the model itself. Therefore, most of these models were only used to interpret the experimental data and analyze the parameter sensitivity. Moreover, the axial variation of liquid dispersion is not well addressed in these models, and the detailed theoretical description of the axial variations of particle diameter and bed voidage is still needed in order to improve the prediction accuracy of the protein adsorption performance in EBA processes.

Recently, we have investigated experimentally and theoretically the axial distribution characteristics of particle size and bed voidage and the axial liquid dispersion behaviors for adsorbents with a normal or lognormal size distribution and with the uniform density (Streamline SP and Streamline DEAE) or the density difference (UpFront Fastline SP) in expanded beds [9–13]. The results showed that nonuniform axial distributions of particle size, bed voidage and liquid dispersion always established in expanded beds with these widely-used adsorbents. We developed several detailed models for describing and predicting the axial variations of these parameters under different conditions. In this work, we present a predicted model for the description of protein adsorption kinetics in EBA taking into account the axial variations of particle diameter, bed voidage, solid–liquid mass transfer coefficient as well as axial liquid dispersion coefficient. The experimental breakthrough data of BSA adsorption on StreamLine DEAE both in this work and in literature and the experimental data of lysozyme adsorption on Streamline SP within different EBA columns and at various conditions reported in the literature will be used to verify the model prediction.

2. Theory

In EBA process, porous adsorbent particles like Streamline series adsorbents are widely used. Thus, we consider the situation of adsorption kinetics using those porous particles here. When target biomolecules in the feedstocks come into an expanded bed, their adsorption and transfer processes include the following aspects: (1) the convective and diffusion mass transfer from liquid phase to adsorbent surfaces, (2) the diffusion within particle pores, and (3) the adsorption at particle surfaces and pore surfaces. These processes are inter-combined and their behaviors are changed with the time along the bed height. Compared to the former two procedures, the surface adsorption process is instantaneous and thus local equilibrium can be assumed in EBA models.

Unlike the general fluidized beds, particles within an expanded bed are classified stably along the bed height. For the case of an equilibrium expansion, each particle takes its own axial position with a little rising or falling due to the plug flow [9,10]. Therefore, the particle mixing is weak in the bed and the axial diffusion of particles can be neglected.

2.1. Hydrodynamics and mass transfer in mobile fluid phase

The present model considers the situation of single target component adsorption within EBA columns. The mass balance equation of target protein in mobile fluid phase is written as [21]

$$\phi(x)\frac{\partial C(x,t)}{\partial t} - \frac{\partial}{\partial x}\left(D_{\mathrm{ax}}(x)\phi(x)\frac{\partial C(x,t)}{\partial x}\right) + U_{\mathrm{L}}\frac{\partial C(x,t)}{\partial x} + \frac{6k_{\mathrm{L}}(x)(C(x,t)-C_{\mathrm{ps}}(x,t))(1-\phi(x))}{d_{\mathrm{s}}(x)} = 0 \quad (1)$$

with the initial condition

$$C(x,t)|_{t=0} = 0 \quad (2)$$

and the boundary conditions

$$C(x,t)|_{x=0} = C_0 + \frac{\phi_0 D_{\mathrm{ax0}}}{U_{\mathrm{L}}}\left.\frac{\partial C(x,t)}{\partial x}\right|_{x=0} \quad (3)$$

$$\left.\frac{\partial C(x,t)}{\partial x}\right|_{x=H} = 0 \quad (4)$$

where C is the bulk-phase concentration of protein, C_0 the inlet concentration of protein, C_{ps} the local equilibrium con-

centration of protein at the external surface of particle, ϕ the local bed voidage, ϕ_0 the inlet bed voidage, D_{ax} the liquid axial dispersion coefficient, D_{ax0} the inlet liquid axial dispersion coefficient, U_L the liquid superficial velocity, k_L the mass transfer coefficient from bulk-phase to external particle surface, d_s the particle diameter, x the distance along the column height and t is the time, respectively.

Considering the axial nonuniformity of liquid dispersion, particle diameter, bed voidage and mass transfer along the bed height, Eq. (1) can be expressed as

$$\phi(x)\frac{\partial C(x,t)}{\partial t} = D_{ax}(x)\phi(x)\frac{\partial^2 C(x,t)}{\partial x^2} - \left(U_L - D_{ax}(x)\frac{d\phi(x)}{dx} - \phi(x)\frac{dD_{ax}(x)}{dx}\right)\frac{\partial C(x,t)}{\partial x} - \frac{6k_L(x)(C(x,t)-C_{ps}(x,t))(1-\phi(x))}{d_s(x)} \quad (5)$$

Based on Eq. (5), for predicting the protein adsorption performance, it is necessary to determine the axial variations of the mean particle diameter, the local bed voidage, the liquid dispersion coefficient, the external mass transfer coefficient as well as the intraparticle mass transfer coefficient along the bed height.

For different kinds of adsorbents, the classification behaviors of adsorbent particles along the bed height under various operation conditions may be different. The mean particle size and the local voidage variations with the axial bed height can be predicted semi-theoretically by taking into account their density and/or size distribution characteristics, as presented detailed elsewhere [9,10]. Here, we consider only the wide-used commercial adsorbent with nearly uniform density and a normal Gaussian size distribution, such as Streamline particles. A brief description of the axial distribution of these particles along an expanded bed is presented as following.

The bulk particle size distribution (by volume) is expressed as [9]

$$f(d_s) = \frac{1}{1 - \int_{-\infty}^{d_{min}} f_1(d_s)\,dd_s - \int_{d_{max}}^{+\infty} f_1(d_s)\,dd_s}\frac{1}{\sqrt{2\pi}\sigma_s} \times \exp\left[-\frac{(d_s - d_{sm})^2}{2\sigma_s^2}\right] \quad (6)$$

where σ_s is the standard deviation of the particle diameters, $f_1(d_s)$ the normal Gaussian probability function and d_{sm}, d_{min} and d_{max} are the averaged, the minimum and the maximum particle diameters, respectively.

For a given particle size distribution and fluid flow conditions, the expanded height $x_{i+1} - x_i$ for particle group with the diameter in the range of $d_s(x_i)$ to $d_s(x_{i+1})$ is given by [9,10]

$$x_{i+1} - x_i = \frac{H_{sb}(1-\phi_{sb})}{1-\phi(x_i)}\int_{d_s(x_i)}^{d_s(x_{i+1})} f(d_s)\,dd_s \quad (7)$$

where the subscript i denotes the ith layer from the bed bottom, $i = 0, 1, 2, \ldots, N$. H_{sb} and ϕ_{sb} are the height and the voidage of the settled bed, $\phi(x_i)$ is the bed voidage in the ith layer. The voidage $\phi(x_i)$ of a certain layer at a given mean particle diameter $d_{sm}(x_i)$ and fluid flow conditions can be calculated as following

$$\frac{18\left[1+8(1-\phi(x_i))^2\right]}{\phi(x_i)^3} + \sqrt{\frac{Ga(x_i)\left[1+8(1-\phi(x_i))\right]}{3\phi(x_i)^3}} = \frac{Ga(x_i)}{Re_s(x_i)} \quad (8)$$

where $Re_s(x_i)$ is Reynolds number in the ith layer given by

$$Re_s(x_i) = \frac{d_{sm}(x_i)U_L\rho_L}{\mu_L} \quad (9)$$

and Galileo number $Ga(x_i)$ in the ith layer is defined by

$$Ga(x_i) = \frac{d_{sm}(x_i)^3 g\left[\rho_s(x_i) - \rho_L\right]\rho_L}{\mu_L^2} \quad (10)$$

and the mean particle diameter $d_{sm}(x_i)$ in the ith layer is given by

$$d_{sm}(x_i) = \frac{d_s(x_i) + d_s(x_{i+1})}{2} \quad (11)$$

Employing these Eqs. (6)–(11), we can get the values of the mean particle diameter and the local bed voidage, as well as their derivatives along the bed height at given operation conditions.

The uniform axial liquid dispersion was frequently assumed in the reported EBA models [16–22], and then the correlations obtained in liquid–solid fluidized beds were always used to determine the axial dispersion coefficient. However, for a stable expanded bed, the axial dispersion coefficient actually varies with the increase of bed height due to the axial variations of particle size, local bed voidage and fluid hydrodynamics. Based on the experimental measurements and the analysis of liquid dispersion mechanisms, the variations of the axial liquid dispersion coefficient along the bed height can be calculated using the correlation obtained by taking into account the contributions of the local bed voidage variations, the interstitial velocity, the liquid and particle properties variations as well as the weak particle movements [12,13].

$$\frac{D_{ax}(x)\rho_L}{\mu_L} = a[Re_s(x)\phi(x)]^b\beta_r(x)^c \quad (12)$$

where μ_L and ρ_L are liquid viscosity and density, a, b and c the empirical parameters depending on the adsorbent used, and β_r is the relative energy dissipation rate. In an expanded bed, the total energy dissipated can be divided into two parts: the energy for suspending the adsorbent particles and the energy for overcoming the column wall resisting force. β_r denotes the ratio of the energy dissipation rate for the wall friction to the total energy dissipation rate, which is used to describe the effect of the particle movements on the axial

dispersion coefficient. Detailed description of β_r has been reported previously [12,13]. In the ith layer, the value of β_r is defined as

$$\beta_r(x_i) = \frac{32U_L}{[d_c^2(\rho_s(x_i) - \rho_L))(1-\phi(x_i))\phi(x_i)g]/\mu_L + 32U_L} \quad (13)$$

where d_c is the inner diameter of column. For Streamline DEAE and SP particles, the values of empirical parameters obtained in our previous experiments [13] are $a = 13.2$, $b = 0.65$ and $c = -0.05$. In the case of $\beta_{ri} = 1$, no particles stay in the column and the axial dispersion will only be a function of Reynolds number. In the case of $\beta_{ri} = 0$, no liquid flow occurs in the column and $D_{axi} = 0$.

The external mass transfer coefficients along the bed height can be calculated as a function of particle Reynolds number and local bed voidage using the correlation reported by Fan et al. [23]

$$\frac{k_L(x)d_s(x)}{D_{AB}} = 2 + 1.5\{Re_s(x)[1-\phi(x)]\}^{1/2}Sc^{1/3} \quad (14)$$

where Sc is Schmidt number ($Sc = \mu_L/D_{AB}\rho_L$) and D_{AB} the molecular diffusion coefficient in the solution.

2.2. Diffusion and adsorption of proteins within adsorbents

For the porous adsorbents, diffusion of proteins within the particle pores can be described using the pore diffusion model [16–22]

$$\phi_p\frac{\partial C_p(x,r,t)}{\partial t} + \frac{\partial q}{\partial t} = D_p\phi_p\left(\frac{\partial^2 C_p(x,r,t)}{\partial r^2} + \frac{2}{r}\frac{\partial C_p(x,r,t)}{\partial r}\right) \quad (15)$$

where C_p is the protein concentration in the particle, ϕ_p the particle porosity, r the radial distance inside the particle, and D_p is the pore diffusion coefficient, which is estimated by the following correlation [24]

$$D_p = \phi_p^2 D_{AB} \quad (16)$$

and q is the adsorbed concentration and for the Langmuir isotherm we have

$$q = \frac{q_{max}C_p(x,r,t)}{K_d + C_p(x,r,t)} \quad (17)$$

where q_{max} is the adsorption capacity and K_d is the dissociation constant.

Substitution of Eq. (17) into Eq. (15) gives

$$\left(\phi_p + \frac{q_{max}K_d}{(K_d + C_p(x,r,t))^2}\right)\frac{\partial C_p(x,r,t)}{\partial t} = D_p\phi_p\left(\frac{\partial^2 C_p(x,r,t)}{\partial r^2} + \frac{2}{r}\frac{\partial C_p(x,r,t)}{\partial r}\right) \quad (18)$$

The initial and boundary conditions are

$$C_p(x,r,t)\big|_{t=0} = 0 \quad (19)$$

$$\left.\frac{\partial C_p(x,r,t)}{\partial r}\right|_{r=0} = 0 \quad (20)$$

$$\phi_p D_p \left.\frac{\partial C_p(x,r,t)}{\partial r}\right|_{r=d_s/2} = k_L(x)(C(x,t) - C_p(x,r,t)\big|_{r=d_s/2}) \quad (21)$$

At a given axial bed position, the nonuniform protein concentration in the radial direction of column is neglected compared with that in the axial direction. Therefore, the local equilibrium concentration of protein at the external surface of particle C_{ps} in Eq. (5) can then be expressed by

$$C_{ps}(x,t) = C_p(x,r,t)\big|_{r=d_s/2} \quad (22)$$

At some given operation conditions and liquid and particle properties, combining Eqs. (1)–(22) gives the closed solution of the adsorption kinetics within an expanded bed.

3. Numerical methods and procedures

With a given liquid superficial velocity, the total expanded bed height and values of the mean particle size, the local bed voidage, the solid–liquid mass transfer coefficient and the axial liquid dispersion coefficient along the bed height were calculated by solving Eqs. (6)–(14) using the method reported in our previous work [9,10]. Then, the obtained values were employed in the solving Eq. (5).

The implicit scheme of finite difference with the backward difference approximation for $\partial C(x,t)/\partial t$ and the central difference approximation for $\partial C(x,t)/\partial x$ and $\partial^2 C(x,t)/\partial x^2$ were adopted to solve Eq. (5), as similar as those used in solving the packed-bed adsorption equations by Özdural et al. [25]. This procedure gave the changes of protein concentration in the mobile phase with the time along the bed height. Fifty finite difference points along the column height were employed in the solving process.

The partial differential within the adsorbent particle as Eq. (18) was solved using the orthogonal collocation method [26–28]. A total of 16 particle radial collocation points were used in the present work. Eq. (18) was discretized at these collocation points leading to a set of ordinary differential equations, which were integrated in the time domain using Runge–Kutta–Gill method. In each time step, solving Eq. (18) gave the values of the protein concentration inside the particle and at the particle surface along the bed height. These values were also employed in the procedure of solving Eq. (5).

4. Experimental

In order to test the predictive model mentioned above, front adsorption experiments combining in-bed sampling

Table 1
Summary of the experimental parameters

C_0 (kg/m^3)	H_{sb} (m)	H (m)	H/H_{sb}	U_L (m/s)
3.0	0.197	0.405	2.06	6.90×10^{-4}
3.0	0.197	0.508	2.58	1.09×10^{-3}
3.0	0.187	0.610	3.26	1.69×10^{-3}
2.0	0.187	0.470	2.51	1.09×10^{-3}
1.0	0.187	0.470	2.51	1.09×10^{-3}

method was employed to get the protein breakthrough curves along the bed height under various operation conditions.

The EBA column used in this work is 80 cm long with inner diameter of 20 mm. The column has a home-made fluid distribution unit at its bottom, a net adapter at its top and 13 sampling ports with about 5 cm intervals along the bed height, as described elsewhere [9–13]. These sampling holes were sealed by moveable rubber bands, which enabled the inserting of the sampling metal needle with its tip covered with mesh. The local breakthrough curves along the bed height were measured by withdrawing the liquid using a peristaltic pump at flow rate of 0.5 ml/min through the needle connected to an on-line flow-through UV spectrometer (Knauer WellChrom spectrophotometer K-2600, Berlin, Germany). The signals of the UV absorbance were fed to an A/D transformer and recorded by a personal computer. Calibration was performed previously to get the relationship between UV signal and protein concentration at the present conditions. Then, the local protein concentrations were calculated from the recorded UV signals based on the calibration relationship. In each run, the measurement was carried out at one port and then the elution, the cleaning-in-place and the bed re-equilibrium were performed before the next run.

The adsorption of BSA from 50 mM NaH_2PO_4/Na_2HPO_4 buffer (pH 7.2, PBS) on Streamline DEAE (Amersham Biosciences, Uppsala, Sweden) was examined. The adsorbent sizes were found to be in the range of about (100–450) $\times 10^{-6}$ m and the mean size is 217×10^{-6} m. The mean density is 1199 kg/m^3 measured using a pycnometer. The temperature in all runs was 298 K. The operation conditions are summarized in Table 1.

5. Results and discussion

The model developed in the present work was applied to predict the breakthrough behaviors of BSA on Streamline DEAE and lysozyme on Streamline SP at different axial positions in expanded beds under various operation conditions. The predicted results were compared with the experimental data obtained in this work and in the literature published [7,9,29].

5.1. BSA adsorption along the bed height

The BSA breakthrough curves at different axial positions under the above mentioned conditions were measured to reveal the adsorption kinetics along the bed height. Fig. 1 shows the experimental results of the BSA breakthrough curves at axial height of 6, 15.5, 25.5 and 45.5 cm. The concentration of BSA in the buffer was 3.0 kg/m^3 and the superficial liquid velocity was 1.09×10^{-3} m/s. As can be seen, the breakthrough curve at the bed height of 6 cm increased sharply with the time. This behavior is affected both by the axial liquid dispersion and the convective mass transfer from liquid to adsorbent particles. In the region from the bed inlet to the bed height of 6 cm, the axial liquid dispersion was relatively intensive, which could induce a broadening of the breakthrough. On the other hand, the local interstitial velocities outside adsorbent particles were high and the convective transfer of protein molecules from liquid to particles was intensive, which correspondingly induced the sharpening of breakthrough curve. Therefore, the observed behavior of the breakthrough curve in this region is a combined result related to both of these two aspects. With the increase of bed height, the curve turned from the bulge-increased to concave-increased shape and the increase degree of breakthrough with time decreased. At a certain breakthrough level, 50% for example, the slope of the breakthrough curves decreased with the increase of bed height. At the bed height of 45.5 cm, the breakthrough concentration increased gradually with the time and it took long time to reach the adsorption balance, which also showed that the influence of the axial liquid dispersion on the adsorption performance existed. This behavior may also be induced by the binding adsorption of BSA molecules onto the adsorbed BSA molecules even the binding sites have been filled, as pointed by Bruce and Chase [7].

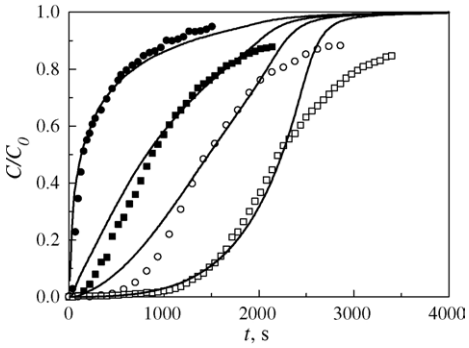

Fig. 1. BSA breakthrough curves at different column heights (Streamline DEAE, $C_0 = 3$ kg/m^3, $U_L = 10.9 \times 10^{-4}$ m/s). (●) $h = 6.0$ cm, (■) $h = 15.5$ cm, (○) $h = 25.5$ cm, (□) $h = 45.5$ cm, and (—) model predicted data.

In Fig. 1, the area between two curves reflects the amount of adsorbed BSA in the corresponding bed zone marked by these two curves. The amount of adsorbed BSA per unit bed volume along the bed height at $C/C_0 = 85\%$ was calculated based on the breakthrough curves. The obtained values were 20.4, 11.0 and 9.8 kg/m^3 in the bed zones of 6–15.5 cm, 15.5–25.5 cm and 25.5–45.5 cm, respectively. Similar decrease trends of the amount of adsorbed BSA per unit bed volume with the increase of bed height were observed at different breakthrough levels. This is because that the local

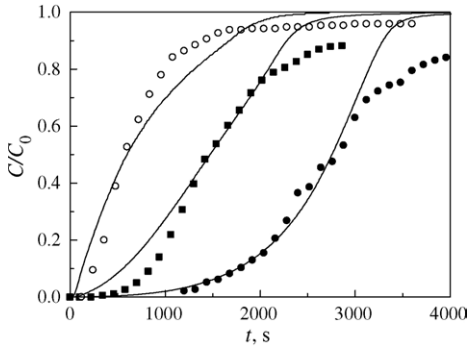

Fig. 2. Effect of superficial liquid velocity on BSA breakthrough (Streamline DEAE, $C_0 = 3\,kg/m^3$, $h = 25.5\,cm$). (●) $U_L = 6.9 \times 10^{-4}$ m/s, (■) $U_L = 10.9 \times 10^{-4}$ m/s, (◯) $U_L = 16.9 \times 10^{-4}$ m/s, and (—) model predicted data.

bed voidage increased with the bed height and the number of adsorbents per unit bed volume then decreased with the increase of the bed height, which caused the decrease of total amount of BSA per unit bed volume along the bed height.

The model mentioned above was employed to predict the breakthrough behaviors at the corresponding column positions and operation conditions. In the model, viscosity and density of the liquid buffer containing BSA were calculated using the equations by Monkos [30]. The diffusion coefficient of BSA in liquid buffer was estimated by the correlation reported by Young et al. [31]. The settled bed voidage for Streamline particles was 0.4 [7]. The particle porosity of Streamline DEAE was 0.85, which was obtained by measuring the volume of water saturated within the particles, i.e. measuring the weights of the given-volume wet and dry particles. For the present experiments, the adsorption capacity and the dissociation constant for BSA on Streamline DEAE were obtained from the experimental data by Bruce and Chase [7]. Parameter values used in the model are summarized in Table 2.

The predicted results were compared with the experimental data and also shown in Fig. 1. It is seen that the model gave a quite good prediction of breakthrough performance in the bed zones with heights of 6–15.5 cm. The model also gave a satisfied prediction in the case that the breakthrough level was lower than 60–80% at the positions of 25.5 and 45.5 cm. When the breakthrough level was higher than 80% in these zones, the model prediction overestimated the breakthrough level with the time. The main reason is that the effect of BSA molecules bound on the previous adsorbent BSA molecules on the adsorption equilibrium was not considered in the present model. The other reason might be that the radial nonuniform distributions of particle size and bed voidage were not included in the present model.

5.2. Influence of liquid velocity on BSA breakthrough

Fig. 2 shows the experimental and predicted breakthrough curves of BSA at the bed height of 25.5 cm under different superficial liquid velocities. The BSA concentration in the

Table 2
Summary of parameters used in the model for BSA on Streamline DEAE

C_0 (kg/m^3)	U_L ($\times 10^{-4}$) (m/s)	H_{sb} (m)	ϕ_{sb}	ϕ_p	ρ_s (kg/m^3)	μ_L ($\times 10^{-3}$) (Pa s)	ρ_L (kg/m^3)	d_{smax} ($\times 10^{-6}$) (m)	d_{smin} ($\times 10^{-6}$) (m)	d_{sm} ($\times 10^{-6}$) (m)	σ_s ($\times 10^{-6}$) (m)	d_c ($\times 10^{-3}$) (m)	D_{AB} ($\times 10^{-11}$) (m^2/s)	D_p ($\times 10^{-11}$) (m^2/s)	K_d (kg/m^3)	q_{max} (kg/m^3)
3.0	6.9	0.197	0.40	0.85	1199	0.9	1002	450	100	217	60	20	6.8	4.9	0.38	56
3.0	10.9	0.197	0.40	0.85	1199	0.9	1002	450	100	217	60	20	6.8	4.9	0.38	56
3.0	16.9	0.187	0.40	0.85	1199	0.9	1002	450	124	217	60	20	6.8	4.9	0.38	56
2.0	10.9	0.187	0.40	0.85	1199	0.9	1002	450	100	217	60	20	6.8	4.9	0.38	56

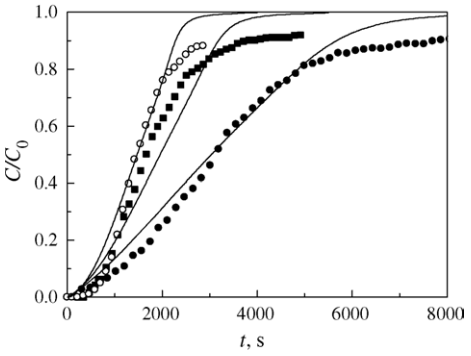

Fig. 3. Effect of feed concentration on BSA breakthrough (Streamline DEAE, $U_L = 1.09 \times 10^{-3}$ m/s, $h = 25.5$ cm). (●) $C_0 = 1$ kg/m^3, (■) $C_0 = 2$ kg/m^3, (◯) $C_0 = 3$ kg/m^3, and (—) model predicted data.

feed buffer was 3.0 kg/m^3 and the superficial liquid velocities were 6.9×10^{-4} m/s, 1.09×10^{-3} m/s and 1.69×10^{-3} m/s, respectively. As can be seen, the model predictions agreed well with most of those experimental data.

From Fig. 2, the breakthrough time for the front reaches the axial position of 25.5 cm at the superficial liquid velocity of 6.9×10^{-4} m/s was about 20 min, which is much longer than that at 1.09×10^{-3} m/s (6 min) or 1.69×10^{-3} m/s (2 min). The amount of adsorbed BSA per unit bed volume at $C/C_0 = 85\%$ was also calculated based on the breakthrough curves. The obtained values were 20.7, 15.9 and 10.5 kg/m^3 in the bed zones of 0–25.5 cm at the superficial liquid velocities of 6.9×10^{-4} m/s, 1.09×10^{-3} m/s and 1.69×10^{-3} m/s, respectively. This indicates that more BSA molecules were adsorbed before breakthrough at the superficial liquid velocity of 6.9×10^{-4} m/s. The reason is not only the lower pass-by velocity, but the influence of particle concentration is also important. Actually, since the expanded bed height increased with the increase of superficial liquid velocity, the total adsorbent volume within the same bed zone (i.e. the region between the bed bottom and the height of 25.5 cm) at the superficial liquid velocity of 6.9×10^{-4} m/s was greater than that at 1.09×10^{-3} m/s or 1.69×10^{-3} m/s, which induced correspondingly more amount of BSA adsorbed. Therefore, the breakthrough time increased with the decrease of superficial liquid velocity.

It is also seen from Fig. 2 that the increasing trend of the breakthrough curve with time was becoming more remarkable with the increase of the superficial liquid velocity. This is probably because that the adsorption effect of BSA molecules bound on other previously adsorbed BSA molecules at the binding sites increased with decrease of superficial liquid velocity.

5.3. Influence of feed concentration on BSA breakthrough

Fig. 3 shows the experimental and predicted breakthrough curves of BSA at the bed height of 25.5 cm under different feed BSA concentrations (1.0, 2.0 and 3.0 kg/m^3). The super-

Table 3
Parameters used in the model prediction

C_0 (kg/m^3)	U_L ($\times 10^{-4}$) (m/s)	H_{sb} (m)	ϕ_{sb}	ϕ_p	ρ_s (kg/m^3)	μ_L ($\times 10^{-3}$) (Pa s)	ρ_L (kg/m^3)	d_{smax} ($\times 10^{-6}$) (m)	d_{smin} ($\times 10^{-6}$) (m)	d_{sm} ($\times 10^{-6}$) (m)	σ_s ($\times 10^{-6}$) (m)	d_c ($\times 10^{-3}$) (m)	D_{AB} ($\times 10^{-11}$) (m^2/s)	D_p ($\times 10^{-11}$) (m^2/s)	K_d (kg/m^3)	q_{max} (kg/m^3)
3.6	6.03	0.206	0.40	0.85	1200	1.0	1002	300	100	200	62	50	6.03	4.35	0.38	56.0
2.0	5.27	0.095	0.40	0.85	1135	0.9	1000	500	90	210	62	25	6.13	4.43	0.06	75.3
1.0	5.27	0.100	0.40	0.85	1135	0.9	1000	500	90	210	62	25	6.13	4.43	0.06	75.3
1.0	8.61	0.095	0.40	0.85	1135	0.9	1000	500	105	210	62	25	6.13	4.43	0.06	75.3
1.0	11.1	0.095	0.400	0.85	1135	0.9	1000	500	130	210	62	25	6.13	4.43	0.06	75.3

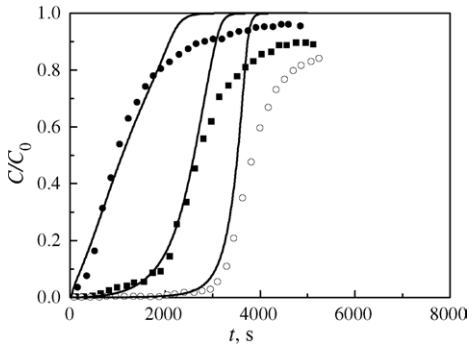

Fig. 4. Comparison of the present model predicted data and the experimental breakthrough curves at different bed heights (Streamline DEAE, $U_L = 6.03 \times 10^{-4}$ m/s, $C_0 = 3.6$ kg/m^3, experimental data from Bruce and Chase [7]). (●) $h = 10$ cm, (■) $h = 25$ cm, (○) $h = 40$ cm, and (—) model predicted data.

ficial liquid velocity was maintained at 1.09×10^{-3} m/s. As can be seen, the model prediction agreed well with experimental data. From the Figure, the lower the feed BSA concentration, the longer time needed to reach the maximum breakthrough level, thus, more feed volume were needed. Moreover, from the areas surrounded by the breakthrough and the C/C_0 axis, the total amounts of BSA absorbed within the bed zone at different feed concentrations were different. The total amount of BSA absorbed at the feed BSA concentration of 3.0 kg/m^3 was greater than that at 2.0 or 1.0 kg/m^3. The corresponding obtained values of the amount of adsorbed BSA per unit bed volume at $C/C_0 = 85\%$ were 15.9, 12.3 and 13.2 kg/m^3. In fact, the concentration gradient of BSA from the bulk liquid within the bed void to the adsorbent surface at the feed BSA concentration of 3.0 kg/m^3 was higher than that at 2.0 or 1.0 kg/m^3, which induced larger mass flux of BSA molecules diffused from liquid to the binding sites within the adsorbent, corresponding more BSA molecules absorbed.

5.4. Comparison of the predicted BSA breakthrough with the experimental data in literature

Bruce and Chase [7] measured the adsorption performance of BSA on Streamline DEAE at the height positions of 10, 25 and 40 cm in a 50 mm inner diameter EBA column. Tong et al. [19] reported the BSA breakthrough curves measured at the bed outlet in a 25 mm inner diameter column under different conditions. Here, we employed the present model to predict the breakthrough behaviors under these two cases. The parameters used in the model are summarized in Table 3. The predicted results were compared with the experimental data from Bruce and Chase [7] and Tong et al. [19], as shown in Figs. 4 and 5 The parameters used in the model are summarized in Table 4. Fig. 6, respectively.

In the calculation, the pore diffusion coefficients in different conditions were estimated by Eq. (16). The obtained values were different from those used in refs. [7,19]. As can be seen, the predicted data by the model agreed quite well with the experimental data of BSA breakthrough from

Table 4
Parameters used in the model prediction of lysozyme on Streamline SP

C_0 (kg/m^3)	U_L ($\times 10^{-4}$) (m/s)	H_{sb} (m)	ϕ_{sb}	ϕ_p	ρ_s (kg/m^3)	μ_L ($\times 10^{-3}$) (Pa s)	ρ_L (kg/m^3)	d_{smax} ($\times 10^{-6}$) (m)	d_{smin} ($\times 10^{-6}$) (m)	d_{sm} ($\times 10^{-6}$) (m)	σ_s ($\times 10^{-6}$) (m)	d_c ($\times 10^{-3}$) (m)	D_{AB} ($\times 10^{-11}$) (m^2/s)	D_p ($\times 10^{-11}$) (m^2/s)	K_d (kg/m^3)	q_{max} (kg/m^3)
1.9	5.94	0.200	0.40	0.85	1184	0.97	1000	400	100	192	51	50	10.4	7.32	0.05	160
4.7	5.11	0.212	0.40	0.85	1184	1.03	1000	400	100	192	51	50	9.74	6.87	0.05	160

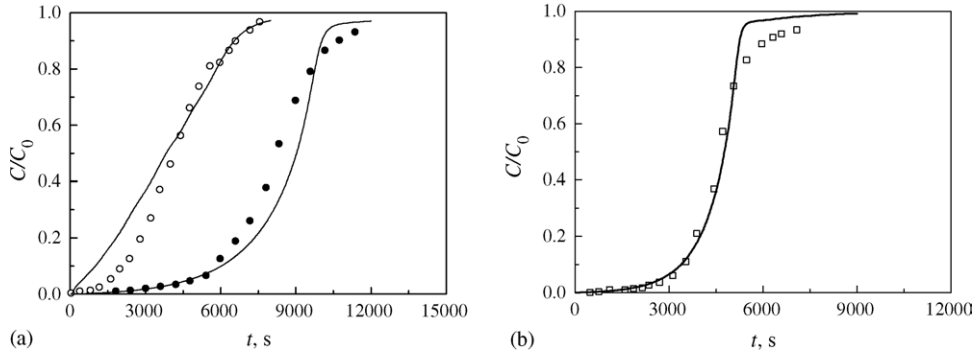

Fig. 5. Comparison of the present model predicted data and the experimental breakthrough curves at different bed heights (Streamline DEAE, experimental data from Tong et al. [18]). (●) $C_0 = 1.0\,kg/m^3$, $U_L = 5.27 \times 10^{-4}$ m/s (◯) $C_0 = 1.0\,kg/m^3$, $U_L = 1.11 \times 10^{-3}$ m/s, (□) $C_0 = 2.0\,kg/m^3$, $U_L = 5.27 \times 10^{-4}$ m/s, and (—) model predicted data.

Bruce and Chase [7] at the heights of 10 and 25 cm. At the height of 40 cm, the model gave a slight overestimation of the breakthrough for $C/C_0 > 60\%$. The reason is as same as that mentioned above for the present work. For the data by Tong et al. [19], the agreement between the model prediction and the experimental measurement was good. Furthermore, it is also seen from these figures that the breakthrough curves become steeper with increasing bed height. This is mainly caused by the combined effects of the axial liquid dispersion and the convective mass transfer, as similar as mentioned in Section 5.1. Actually, the axial liquid dispersion and the convective mass transfer were not uniform but changed along the bed height. In the bottom region near the bed inlet, the intensive axial liquid dispersion broadened the breakthrough, while the high convective mass transfer of proteins from liquid to particles sharpened the breakthrough curves. With the increase of bed height, the axial dispersion became lower, which induced the decrease of broadening of breakthrough. On the other hand, the interstitial velocity decreased gradually with increasing of bed height, which induced the decrease of the convective mass transfer and correspondingly decreased the sharpening of breakthrough. The observed breakthrough behaviors are caused by the combining of these aspects. Those are just the reasons that the axial nonuniform liquid dispersion was taken into account in the present work for describing special breakthrough properties in expanded bed, and the experimental results verified the modeling work well.

5.5. Model prediction of lysozyme breakthrough and compared with literature data

The model prediction of lysozyme adsorption on Streamline SP under the conditions reported by Bruce and Chase [7] and Bruce et al. [29] were conducted. In the model, the viscosity and the density of liquid buffer with lysozyme were calculated based on ref. [32]. The diffusion coefficient of lysozyme in liquid buffer was calculated by the correlation presented by Young et al. [31]. The adsorbent porosity of Streamline SP obtained in our measurements was 0.84. The adsorption capacity and the dissociation constant for lysozyme on Streamline SP were obtained from literature [33]. shows the experimental and calculated lysozyme breakthrough curves at different bed heights. It is seen that the predicted values agreed well with those measured results.

Although the distributors used in the present work and in the literature were different, the model still gave satisfied prediction of BSA or lysozyme breakthrough. This demonstrated that the model developed here is suitable to describe the general proteins adsorption behaviors in EBA columns. How-

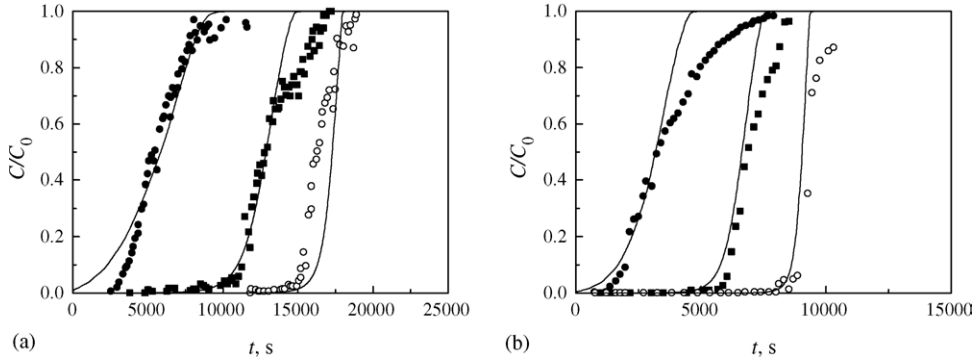

Fig. 6. Comparison of the predicted data and the experimental breakthrough curves at different bed heights (Streamline SP, experimental data from Bruce and Chase [7] and Bruce et al. [28]). (●) $h = 10$ cm (◯) $h = 25$ cm (□) $h = 40$ cm, and (—) model predicted data.

ever, the present work only considers the proteins adsorption performance from liquors without cells or cell debris and, thus the effects of these solids on the axial liquid dispersion, particle classification as well as bed voidage variation were ignored. For the feedstocks with cells and cell debris, the adsorption performance should be further addressed and the model is needed to be improved by taking into account the influence of cells or cell debris.

6. Conclusions

The adsorption behaviors of proteins along bed height in expanded beds are particular and quite complex, which is influenced by several operation factors such as liquid velocity and feed concentration. The axial nonuniform liquid dispersion and particle classification should be taken into account for accurate description of protein adsorption in expanded bed. By considering the axial variations of adsorbent particle diameter, liquid dispersion, bed voidage and target component mass transfer, the model developed in the present work is effective in predicting the protein adsorption along the bed height under different situations. Compared with the experimental data obtained in this work and reported in the literature, the present model give a good prediction of breakthrough behaviors for BSA on Streamline DEAE and lysozyme on Streamline SP along the bed height in different expanded bed columns under various conditions, which verifies that the model describes a general situation of protein adsorption performance in expanded beds. However, the effects of cells or cell debris are not considered in the present model. It is still a challenge to apply this model in describing the adsorption of target biomolecules from real feedstocks with cells and cell debris. A more comprehensive model is expected in future.

7. Nomenclature

a, b, c	empirical parameters in Eq. (12)
C	bulk-phase concentration of protein (kg/m^3)
C_0	inlet concentration of protein (kg/m^3)
C_p	protein concentration in the particle (kg/m^3)
C_{ps}	equilibrium concentration of protein at external surface of particle (kg/m^3)
d_c	inner diameter of column (m)
d_{max}	maximum particle diameter (m)
d_{min}	minimum particle diameter (m)
d_s	particle diameter (m)
$d_s(x_i)$	mean particle diameter in the ith layer (m)
d_{sm}	mean particle diameter (m)
D_{AB}	molecular diffusion coefficient (m^2/s)
D_{ax}	axial dispersion coefficient (m^2/s)
D_{az0}	inlet liquid axial dispersion coefficient (m^2/s)
D_p	pore diffusion coefficient (m^2/s)
$f(d_s)$	particle size distribution function (by volume)
$f_1(d_s)$	normal Gaussian probability function
g	gravitational acceleration (m/s^2)
$Ga(x_i)$	Galileo number in the ith layer defined by Eq. (10)
H	axial bed height (m)
H_{sb}	settled bed height (m)
k_L	mass transfer coefficient (m/s)
K_d	dissociation constant (kg/m^3)
q	adsorbed concentration (kg/m^3)
q_{max}	adsorption capacity (kg/m^3)
r	radial distance inside the particle (m)
$Re_s(x_i)$	Reynolds number in the ith layer defined by Eq. (9)
Sc	Schmidt number, $Sc = \mu_L/D_{AB}\rho_L$
t	time (s)
U_L	superficial liquid velocity (m/s)
x	distance along the column height (m)

Greek letters

β_r	ratio of energy dissipation rate for wall friction to total energy dissipation rate
ϕ	local voidage
ϕ_0	inlet bed voidage
ϕ_p	particle porosity
ϕ_{sb}	settled bed voidage
μ_L	liquid viscosity (Pa s)
ρ_L	liquid density (kg/m^3)
$\rho_s(x_i)$	particle density in the ith layer (kg/m^3)
ρ_s	mean particle density (kg/m^3)
σ_s	standard deviation of particle size (m)

Acknowledgments

The support of the National Natural Science Foundation of China (No. 20206029) is gratefully acknowledged. The authors are grateful to the research support from Zhejiang Province Foundation for post-doctors. We also want to thank the German Academic Exchange Service (DAAD) for the instrument donation of Spectrophotometer K2600.

References

[1] H.A. Chase, Trends Biotechnol. 12 (1994) 296.
[2] R. Hjorth, Trends Biotechnol. 15 (1997) 230.
[3] J. Thömmes, Adv. Biochem. Eng. 58 (1997) 185.
[4] F.B. Anspach, D. Curbelo, R. Hartman, G. Garke, W.D. Deckwer, J. Chromatogr. A 865 (1999) 129.
[5] A. Karau, C. Benken, J. Thömmes, M.R. Kula, Biotechnol. Bioeng. 55 (1997) 54.
[6] N.A. Willoughby, R. Hjorth, N.J. Titchener-Hooker, Biotechnol. Bioeng. 69 (2000) 649.
[7] L.J. Bruce, H.A. Chase, Chem. Eng. Sci. 56 (2001) 3149.
[8] X.D. Tong, Y. Sun, J. Chromatogr. A 977 (2002) 173.
[9] J.X. Yun, S.J. Yao, D.Q. Lin, M.H. Lu, W.T. Zhao, Chem. Eng. Sci. 59 (2004) 449.
[10] J.X. Yun, D.Q. Lin, M.H. Lu, L.N. Zhong, S.J. Yao, Chem. Eng. Sci. 59 (2004) 5873.

[11] J.X. Yun, D.Q. Lin, S.J. Yao, in: Z. Tong, S.H. Kim (Eds.), Frontiers on Separation Science and Technology, World Scientific Publ. Co. Pte. Ltd., Singapore, 2004, p. 964.
[12] J.X. Yun, D.Q. Lin, S.J. Yao, Ind. Eng. Chem. Res. 43 (2004) 8066.
[13] J.X. Yun, S.J. Yao, D.Q. Lin, Chem. Eng. J. 109 (2005) 123.
[14] D.J. Wiblin, S.D. Roe, R.G. Myhill, J. Chromatogr. A 702 (1995) 81.
[15] L.J. Bruce, H.A. Chase, Chem. Eng. Sci. 57 (2002) 3085.
[16] P.R. Wright, B.J. Glasser, AIChE J. 47 (2001) 474.
[17] X.D. Tong, X.Y. Dong, Y. Sun, Biochem. Eng. J. 12 (2002) 117.
[18] W.D. Chen, X.Y. Dong, Y. Sun, J. Chromatogr. A 1012 (2003) 1.
[19] X.D. Tong, B. Xue, Y. Sun, Biochem. Eng. J. 16 (2003) 265.
[20] P. Li, G.H. Xiu, A.E. Rodrigues, Chem. Eng. Sci. 59 (2004) 3837.
[21] K. Kaczmarski, J.C. Bellot, Biotechnol. Prog. 20 (2004) 786.
[22] K. Kaczmarski, J.C. Bellot, J. Chromatogr. A 1069 (2005) 91.
[23] L.S. Fan, Y.C. Yang, C.Y. Wen, AIChE J. 6 (1960) 482.
[24] K. Miyabe, G. Guiochon, J. Chromatogr. A 866 (2000) 147.
[25] A.R. Özdural, A. Alkan, P.J.A.M. Kerkhof, J. Chromatogr. A 1041 (2004) 77.
[26] J.V. Villadsen, W.E. Stewart, Chem. Eng. Sci. 22 (1967) 1483.
[27] J. Villansen, M.L. Michelsen, Solution of Differential Equation Models by Polynomial Approximation, Prentice-Hall Inc., New Jersey, 1978.
[28] B.A. Finlayson, Nonlinear Analysis in Chemical Engineering, McGraw-Hill Inc., New York, 1980.
[29] L.J. Bruce, R.H. Clemmitt, D.C. Nash, H.A. Chase, J. Chem. Technol. Biotechnol. 74 (1999) 264.
[30] K. Monkos, Int. J. Biol. Macromol. 18 (1996) 61.
[31] M.E. Young, P.A. Carroad, R.L. Bell, Biotechnol. Bioeng. 22 (1980) 947.
[32] K. Monkos, Biochim. Biophys. Acta 1339 (1997) 304.
[33] X.Y. Zhao, X.D. Tong, Y. Sun, Chinese J. Process Eng. 4 (2004) 103.